COLLISION DYNAMICS

Tomography of Feshbach resonance states

Baruch Margulis[1], Karl P. Horn[2], Daniel M. Reich[2], Meenu Upadhyay[3], Nitzan Kahn[1], Arthur Christianen[4,5], Ad van der Avoird[5], Gerrit C. Groenenboom[5], Markus Meuwly[3]*, Christiane P. Koch[2]*, Edvardas Narevicius[1,6]*

Feshbach resonances are fundamental to interparticle interactions and become particularly important in cold collisions with atoms, ions, and molecules. In this work, we present the detection of Feshbach resonances in a benchmark system for strongly interacting and highly anisotropic collisions: molecular hydrogen ions colliding with noble gas atoms. The collisions are launched by cold Penning ionization, which exclusively populates Feshbach resonances that span both short- and long-range parts of the interaction potential. We resolved all final molecular channels in a tomographic manner using ion-electron coincidence detection. We demonstrate the nonstatistical nature of the final-state distribution. By performing quantum scattering calculations on ab initio potential energy surfaces, we show that the isolation of the Feshbach resonance pathways reveals their distinctive fingerprints in the collision outcome.

In atomic and molecular collisions, elastic, inelastic, and reactive scattering compete with resonance pathways. In particular, Feshbach scattering resonances that arise from the coupling between different degrees of freedom are instrumental for the transfer of energy from internal to relative motion (*1*, *2*). Feshbach resonances have been observed in atom-atom (*3*–*5*), atom-ion (*6*), atom-molecule (*7*–*9*), bimolecular (*10*, *11*), and field-dressed bimolecular collisions (*12*) by tuning either the collision energy or the magnetic field strength in the case of trapped ultracold particles. Alternatively, a single resonance path can be selected by spectroscopic excitation, as in predissociation (*13*–*16*) or electron photodetachment (*17*, *18*). However, one is then limited to the Franck-Condon region close to the equilibrium geometry that represents a rather small part of the overall phase space. In this work, we combined the advantage of ultracold molecular collisions exploring a large part of the phase space with the preparation of isolated resonances that allowed us to follow collision pathways. We achieved this by populating vibrational Feshbach resonances at long range, just below the threshold. In contrast with predissociation and similar to full collisions, the colliding particles possess a set of well-defined, unperturbed internal quantum numbers. As in reactive bialkali systems (*7*, *9*, *19*), we explored the collision regime where the short range intermolecular interaction is strong, leading to the mixing between tens of rovibrational quantum states coupled by anisotropic interactions.

Our method is complementary to and expands the capabilities of electron photodetachment spectroscopy (EPDS) (*17*, *18*) (supplementary materials). In EPDS, the electron is stripped away from an anion through interaction with laser radiation. The electron kinetic energy distribution contains information about the energy levels of the neutral product. However, the detection of subsequent dynamics is challenging. In our method, the starting point is a cold collision between an electronically excited atom and a neutral molecule. The electron is emitted during a charge transfer process that results in ionic molecular products with a well-defined set of internal quantum numbers. Because of the low collision energy, we populated a narrow momentum band during the ionization step. In such a case, the distribution of initial and final molecular ion states can be simply detected through energy conservation. The kinetic energy distribution of the molecular ions provides additional information that encodes the final quantum-state distribution resulting from the decay of Feshbach resonances populated upon the ionization step. The nonselective nature of the ionization process leads to the formation of molecular ions in many vibrational states. As a result, the ionic kinetic energy distribution contains contributions from all the accessible vibrational branches of Feshbach resonances. We disentangled the contribution of individual initial molecular ionic states using ion-electron coincidence detection. This scheme allowed us to simultaneously detect all the possible quantum states in a tomographic manner. Our results show that each Feshbach resonance has a distinctive signature reflected in the final quantum-state distribution. In a similarly strongly interacting system, it has been shown (*20*) that the final-state distribution foll statistical arguments. In earlier reactive scat ing experiments in which Feshbach resonances were detected (*21*, *22*), the measured final-state distribution was found to be insensitive to the collision energy up to 180 K and did not depend on the total angular momentum (*23*). By contrast, in our case, the quantum signatures of vibrational resonances are sensitive to the details of the interaction. We confirmed this by carrying out full ab initio–based quantum scattering calculations for the benchmark system of H_2^+ colliding with a noble gas atom. Our work shows that quantum signatures can be observed even in strongly interacting and anisotropic systems if the resonance pathway can be isolated.

The method

We present a schematic description of our approach in Fig. 1. The starting point is the collision between a metastable noble gas atom and a ground-state molecule, which leads to Penning ionization (PI). The ionization is a sudden, nonadiabatic transition of the initial neutral state onto the manifold of ionic states (*24*). It can be described by projecting the scattering wave function of the neutrals Ψ (R), scaled by the ionization probability Γ (R), onto the full set of states describing the molecular ion–neutral atom interactions. Because ionization occurs at large intermolecular distances, the initial state is projected in the region where the long-range part of the intermolecular potential dominates. As a result, the Feshbach states are characterized by the free molecule basis with no change in the rotational quantum number (j) of the molecule. The populated states differ asymptotically by the vibrational energy of the molecular ion. Because of the electron's small mass, it carries away most of the excess energy released at the ionization step. Therefore, the initial vibrational state (v) of the molecular ion is encoded in the electron kinetic energy. The energy distribution of electrons represents the vibrational spectrum of the molecular ion with near Franck-Condon probabilities (*25*, *26*). In Fig. 1B, we show the resulting dynamics of such a Feshbach resonance state in which a single quantum of vibrational excitation is converted into a combination of kinetic and rotational energy. In this system, the closed channel is the vibrationally excited state, whereas the open channels are the vibrationally ground, rotationally excited states. The final quantum-state distribution is reflected in the velocity distribution of the molecular ion. The electron-ion coincidence measurement completes the quantum state-to-state mapping because every detected electron-ion pair is generated during the same collision event.

The ionization step is governed by a charge transfer process that depends exponentially

---

[1]Department of Chemical and Biological Physics, Weizmann Institute of Science, Rehovot 7610001, Israel. [2]Dahlem Center for Complex Quantum Systems and Fachbereich Physik, Freie Universität Berlin, Arnimallee 14, 14195 Berlin, Germany. [3]Department of Chemistry, University of Basel, Basel, Switzerland. [4]Max-Planck-Institut für Quantenoptik, Hans-Kopfermann-Strasse 1, D-85748 Garching, Germany. [5]Theoretical Chemistry, Institute for Molecules and Materials, Radboud University, Heyendaalseweg 135, 6525 AJ Nijmegen, Netherlands. [6]Department of Physics, Technische Universität, Dortmund, Germany.
***Corresponding author. Email: edvardas.narevicius@tu-dortmund.de (E.N.); m.meuwly@unibas.ch (M.M.); christiane.koch@fu-berlin.de (C.P.K.)**

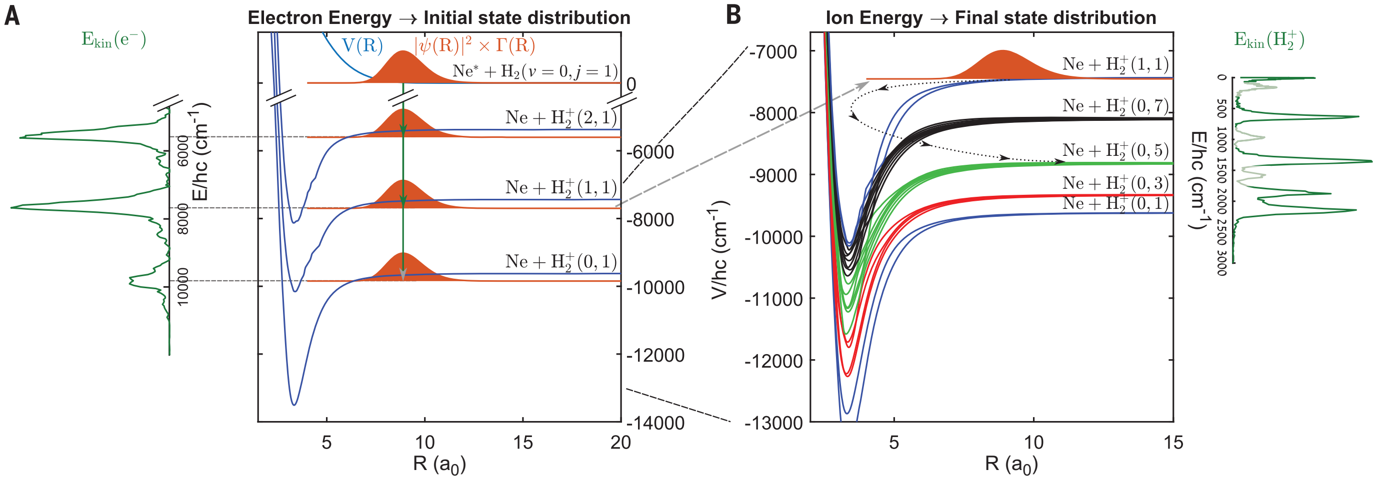

Fig. 1. Adiabatic potential energy curves and wave functions describing Penning collisions at total angular momentum state J = 6 and partial wave l = 5 between metastable neon and ortho-H_2 in its ground rovibrational state. Each adiabatic curve corresponds to the vibrational and rotational quantum numbers (v, j), of H_2^+. R, intermolecular separation in Bohr radii (a_0). Same-color curves indicate adiabatic curves with different partial wave quantum number l, but with the same molecular rotation quantum number j. (**A**) Representation of the ionization step. The green curve represents the measured kinetic energy (E) of electrons and provides the initial-state distribution of the Feshbach states. The energy positions of the projected states are set relative to the center of the measured peaks. (**B**) Representation of the decay of Feshbach states formed upon ionization. The measured ionic kinetic energy distribution (green curve) corresponds to the final-state distribution. The contribution of para-H_2 to the kinetic energy distribution is indicated in light green. The energy position of the projected state is set by the measured resonance energy. *hc*, Planck constant times the speed of light.

Fig. 2. Computational characteristics of Feshbach resonance states. (**A**) Zoomed-in view of adiabatic PES together with corresponding radial wave functions Ψ (R). Shown on the right side of the figure are computed overlap plots for total angular momentum J = 6 and initial partial wave l = 5, which represent the energy distribution of populated Feshbach states. The presented ionic energy eigenstates have the largest overlap with the initial neutral state, which describes the Penning collisions, $|\Psi(R)|^2 \times \Gamma(R)$. (**B**) Relative contribution of each angular momentum state of collision for Ne(^{3}P)-ortho-H_2 collisions considering the experimental collision energy and spread. P(l,J), ionization probability per initial l and J. (**C**) Computed ionic energy distributions that represent final-state distribution corresponding to initial vibrational states v = 2 and v = 1. The threshold energies are labeled by the final rotational state of free ortho $-$ H_2^+ ions. The distributions are normalized to unity. $P(E)$, probability as a function of energy, E; *Arb. u.*, arbitrary units.

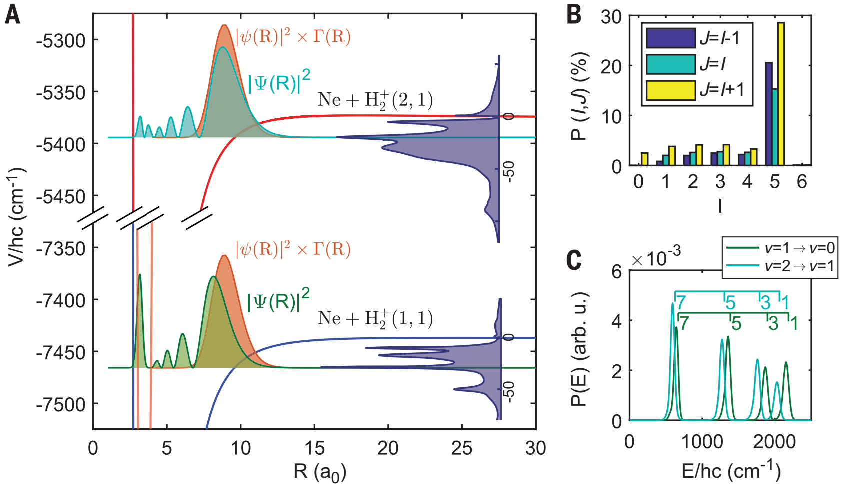

on the intermolecular distance. As such, the part of the scattering wave function that undergoes ionization is strongly localized in the vicinity of the classical turning point of the neutral potential energy surface (Fig. 1A). Such a strong localization of the initial wave function is essential for the resolution of our measurement because it determines the energy spread in the distribution of populated ionic states. After ionization, the initial scattering wave function spans a narrow, 50-cm^{-1}-wide energy band located 30 cm^{-1} away from the dissociation threshold of the molecular ion–neutral atom interaction potential energy surface. This energy window constitutes a small fraction of the total interaction strength reflected by a deep potential well of 4450 cm^{-1} in the case of $Ne - H_2^+$. This energy window contains only a few Feshbach resonances, associated to triatomic rovibrational states (Shown in Fig. 2A for two initial vibrational states, v = 2 and v = 1, of the molecular hydrogen ion). Moreover, the total angular momentum and parity of the Feshbach resonance are set during the PI step. By tuning the collision energy of the neutral collision system to match a shape resonance, we were able to control the total angular momentum distribution, which peaked around the resonant partial wave (*27*, *28*). Notably, the near-threshold Feshbach resonance wave functions are sensitive to both the short- and the long-range parts of the interaction potential. While in the short range, all of the degrees of freedom are strongly coupled by the anisotropy of the potential energy surface (PES), the resonance wavefunction at large separation is nearly separable into the molecular ion and neutral atom. Whereas the strength of the leading term of the anisotropic interaction is 1300 cm^{-1} at an intermolecular separation of 2 a_0, it falls to 1 cm^{-1} at 10 a_0. We demonstrate that each Feshbach resonance state has a distinctive signature in the final-state distribution depending on the Feshbach state energy,

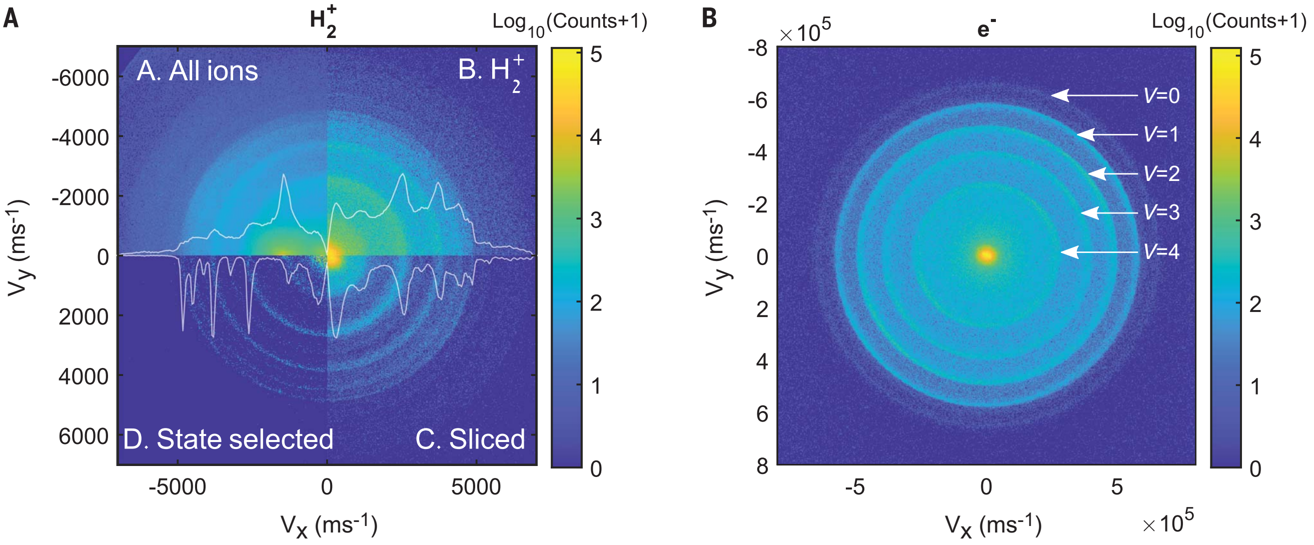

Fig. 3. VMI images of ions and coincidence electrons. (**A**) In clockwise order from the top left corner of the image, the first quadrant presents the overall accumulated ionic VMI image, which includes all ionic masses; the second quadrant shows the VMI image of H_2^+ ions alone, obtained with electron-ion coincidence; the third quadrant presents a sliced image using ion time-of-flight information; and the last quadrant presents the sliced VMI image of ions related to initial vibrational state v = 1 with ion-electron correlations. Angle-integrated velocity distributions are indicated with white curves at each quadrant. (**B**) VMI image of coincidence electrons corresponding to H_2^+.

the total angular momentum, and the vibrational quantum number (Fig. 2C).

Results and discussion

We studied two benchmark molecular ion collision systems, $Ne - H_2^+$ and $He - H_2^+$, by measuring the correlated energy distributions of the products of Ne*-H_2 and He*-H_2 PI collisions. The experimental setup is described in (*29*). In short, we generated two supersonic beams of metastable noble gas atoms and ground-state molecules using two Even-Lavie (*30*) valves that were positioned at a relative angle of 4.5°. We excited the noble gas atoms to a metastable state by means of a dielectric discharge that was located directly after the valve orifice (*31*). We determined the beam mean velocity by the valve temperature and the gas mixture composition. We performed PI collisions at an energy that matched the position of one of the shape resonances that occur at a few Kelvin (*27*). We first located the shape resonance positions with a complementary measurement by using the merged beam approach (supplementary materials). We present the angular momentum–state distribution for Ne*-ortho-H_2 and Ne*-para-H_2 and He*-H_2 collisions in Fig. 2B and fig. S2, respectively. For Ne*+H_2, we chose a collision energy that matches the position of the $l = 5$ shape resonance. As a result, scattering states with total angular momenta J = 4, 5, and 6 had the highest contribution.

We detected the product ion and electron velocities using a coincidence double velocity map imaging apparatus (*29*). Coincidence detection was the most important aspect of our experiment. The correlation between ions and electrons allowed us to extract the mass, identify the initial state, and determine the velocity magnitude distribution instead of just the projection. It also allowed us to correct the ionic velocity map imaging (VMI) images for electron recoil. Such a correction was essential for He-H_2 where the electron recoil blurred the ionic VMI image by about 100 m/s.

We present the ion and electron VMI images as measured in coincidence during the Ne*-H_2 collisions in Fig. 3. The ion VMI image is divided into quadrants that represent the various steps in the analysis of the raw, accumulated data. We started with the raw accumulated VMI image, which includes all of the ionic products in Fig. 3A. We used time-of-flight (TOF) information to obtain the VMI image of H_2^+ ions alone (Fig. 3B). During the next step, we selected the central part of H_2^+ TOF distribution to time-slice the VMI image (Fig. 3C). This procedure enabled us to construct the velocity-magnitude distribution by means of angle integration of a sliced image without the need of inverse Abel transformation–based techniques. The mass-selected and time-sliced ionic VMI image consists of a series of concentric rings indicating a set of discrete final quantum state channels in which the internal vibrational molecular ion energy is converted into a combination of the final rovibrational state and translational energy. However, this image contains information from all of the five initial vibrational states of the H_2^+ molecular ion that are populated during the quenching process. We constructed the ionic VMI image that corresponds to an individual initial quantum state of H_2^+ by postselecting only those ions that correlate with the electrons within a certain kinetic energy window. Our tomography procedure required us to eliminate the effect of high-energy electrons on rings associated with the lower-energy electrons. We have developed a "peeling" algorithm that corrects an individual ionic image because of the overlap of its coincidence electrons with higher-energy electrons. A detailed description of the peeling algorithm can be found in the supplementary materials.

We obtained the energy distribution of the molecular ions by angular integration of the sliced, initial state–selected VMI images (Fig. 4, blue curves). The energy scale corresponds to the kinetic energy release, E, which was partitioned between the molecular ion and the neutral atom according to momentum conservation. We observed sharp peaks indicating the quenching of Feshbach resonances to different continuum states that were labeled by the final quantum state (v', j') of the free molecular ion. The final-state distribution thus represents the observation of the projection of the Feshbach resonance onto the continuum-basis set, which we refer to as tomography. The threshold energies are depicted in Fig. 4 with black and green lines for Δv = 1 and Δv = 2 transitions, respectively. Each threshold energy is labeled by the final rotational state, j', of the free H_2^+ ion. We observed a higher probability of odd final

Fig. 4. Experimental and theoretical kinetic energy distributions that show the decay of Feshbach states into various continuum states. (**A** and **B**) $\mathrm{Ne}-\mathrm{H}_2^+$ at (A) $v = 1$ and (B) $v = 2$. (**C** and **D**) $\mathrm{He}-\mathrm{H}_2^+$ at (C) $v = 1$ and (D) $v = 2$. Theoretical curves are convoluted by the experimental resolution. Experimental and theoretical kinetic energy distributions indicated with blue and red curves, respectively. Distributions based on the statistical model are indicated with the pink dashed curves. *Arb. u.*, arbitrary units.

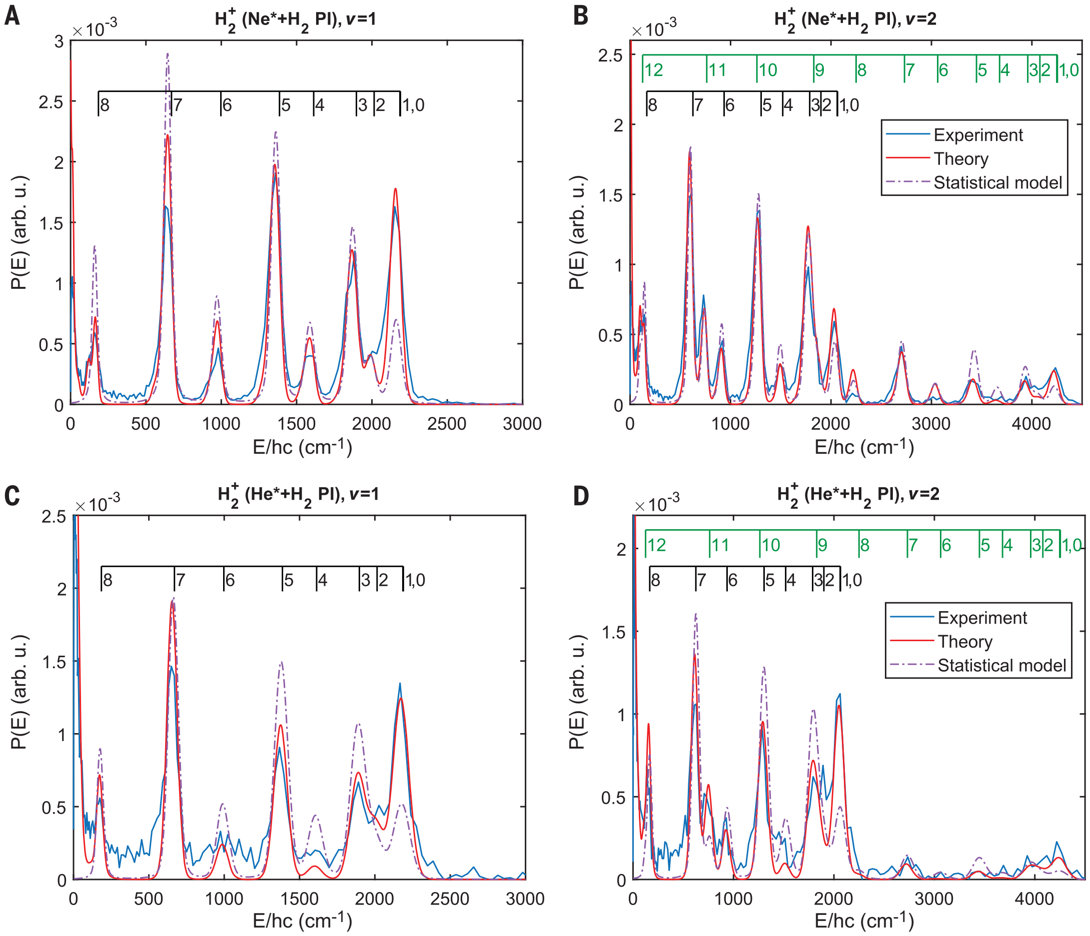

rotational states because of the spin statistics of ortho- versus parahydrogen spin isomers with the 3:1 statistical population ratio. In addition to the resonance state tomography, we obtained the resonance energy that is reflected by the shift of all peaks relative to the threshold energies. For the $v = 1$ state, we found the mean resonance energies to be $-28.9 \pm 3.6\ \mathrm{cm}^{-1}$ for $\mathrm{Ne}-\mathrm{H}_2^+$ and $-20.8 \pm 3.1\ \mathrm{cm}^{-1}$ for $\mathrm{He}-\mathrm{H}_2^+$. We report all resonance energies relative to the position of the noble gas atom and rotational ground-state molecule dissociation threshold.

To confirm the nature of the resonances and to provide additional characterization, we carried out quantum wave packet calculations on an available full configuration interaction (FCI) PES for $\mathrm{He}-\mathrm{H}_2^+$ (*32*) and a new PES for $\mathrm{Ne}-\mathrm{H}_2^+$. We determined the new $^2A'$ $\mathrm{Ne}-\mathrm{H}_2^+$ PES using 38,200 reference energies at the coupled-cluster single-, double-, and perturbative triple-excitations [CCSD(T)]/aug-cc-pV5z level of theory. We performed full coupled-channel calculations of the $\mathrm{He}-\mathrm{H}_2^+$ and $\mathrm{Ne}-\mathrm{H}_2^+$ cross sections with converged bases, with rotational states going up to and including $j = 25$ and vibrational states going up to and including $v = 5$, respectively. For $\mathrm{He}-\mathrm{H}_2^+$, fewer rotational states were required to obtain convergence. The numerical results were convoluted with the experimental uncertainty and are in excellent agreement with the experimental data (Fig. 4, blue versus red traces). Together with earlier work on the near-dissociative states of $\mathrm{He}-\mathrm{H}_2^+$ (*32*), the present agreement between experiment and theory points to near-spectroscopic accuracy of the FCI PES. Similarly, for $\mathrm{Ne}-\mathrm{H}_2^+$, the agreement between computational and experimental results is very encouraging. Further improvement could be obtained from morphing the underlying PES (*33*, *34*).

Because of the strong and highly anisotropic intermolecular interaction, one could expect a statistical description to be sufficient to describe the final-state distribution. Both interaction strength and anisotropy are comparable to the case of KRb + KRb bimolecular reactions (*20*). In the bimolecular case, we found deviations from the statistical model at the limit of the reaction exothermicity at which the centrifugal barrier hinders the reaction rate. In our case, the level of initial excitation relative to the centrifugal barrier height in the exit channel (Fig. 1B) allows all vibrational and rotational transitions to occur. In a purely statistical approach, the decay probability is proportional to the number of energetically accessible exit channels (*20*, *35*). The level of degeneracy in each continuum state is set by the initial total angular momentum J and by parity $(-1)^{j+l}$, which are conserved quantities. For a final rotational state j', the number of exit channels is determined by the number of available partial waves that fulfill the relation $J = |j' - l'|, |j' - l'| + 1, \ldots, j' + l'$ and maintain the right parity. We have constructed a statistical model in which we assumed a single Feshbach resonance, at position and width obtained with exact calculations, for which the decay probability to each final rovibrational state is given by the number of allowed partial waves. The resulting energy distribution was convoluted by the experimental resolution and is shown as pink dashed lines in Fig. 4. Comparing the results of this procedure to the experimental data shows clear deviations from the statistical model. We show a quantitative comparison of the results of the statistical model and exact calculations to the experimental data in fig. S10. In particular, the statistical model underestimates the decay to states with low final j' and overestimates the decay to states with high final j'. This observation suggests that certain transition probabilities are preferred rather than statistical.

Outlook

Although we probed a collision system with strong interactions (charge-induced dipole) and high anisotropy, the Feshbach resonance states have a distinct quantum signature in the final-state distribution. This property may be useful for control over the final-state distribution by manipulating the quantum state of the Feshbach state itself. One way to do so is by tuning the total angular momentum, which is difficult to control. However, an effective way to select states with a certain amount of total angular momentum is to leverage different shape resonances of the neutral collision complex. This could be done with the merged beam approach, in which collision dynamics could be tuned down to a single quantum of angular momentum (*36*). Performing coincidence experiments in the *p*-wave limit will demonstrate the control of the final-state distribution. Moreover, because of the reduction in participating quantum states, individual Feshbach states that correspond to the triatomic rovibrational spectrum could be resolved.

REFERENCES AND NOTES

1. H. Feshbach, *Ann. Phys.* **5**, 357–390 (1958).
2. U. Fano, *Phys. Rev.* **124**, 1866–1878 (1961).
3. A. Frisch *et al.*, *Nature* **507**, 475–479 (2014).
4. V. Barbé *et al.*, *Nat. Phys.* **14**, 881–884 (2018).
5. C. Chin, R. Grimm, P. Julienne, E. Tiesinga, *Rev. Mod. Phys.* **82**, 1225–1286 (2010).
6. P. Weckesser *et al.*, *Nature* **600**, 429–433 (2021).
7. H. Son *et al.*, *Science* **375**, 1006–1010 (2022).
8. T. de Jongh *et al.*, *Science* **368**, 626–630 (2020).
9. H. Yang *et al.*, *Science* **363**, 261–264 (2019).
10. J. J. Park, Y.-K. Lu, A. O. Jamison, T. V. Tscherbul, W. Ketterle, *Nature* **614**, 54–58 (2023).
11. S. Chefdeville *et al.*, *Science* **341**, 1094–1096 (2013).
12. X.-Y. Chen *et al.*, *Nature* **614**, 59–63 (2023).
13. F. F. Crim, *Science* **249**, 1387–1392 (1990).
14. R. E. Miller, *Science* **240**, 447–453 (1988).
15. A. Rohrbacher, N. Halberstadt, K. C. Janda, *Annu. Rev. Phys. Chem.* **51**, 405–433 (2000).
16. C. D. Foley, C. Xie, H. Guo, A. G. Suits, *Science* **374**, 1122–1127 (2021).
17. J. B. Kim *et al.*, *Science* **349**, 510–513 (2015).
18. R. Otto *et al.*, *Science* **343**, 396–399 (2014).
19. K.-K. Ni *et al.*, *Science* **322**, 231–235 (2008).
20. Y. Liu *et al.*, *Nature* **593**, 379–384 (2021).
21. R. T. Skodje *et al.*, *Phys. Rev. Lett.* **85**, 1206–1209 (2000).
22. M. Qiu *et al.*, *Science* **311**, 1440–1443 (2006).
23. T. Wang *et al.*, *J. Phys. Chem. Lett.* **5**, 3049–3055 (2014).
24. W. H. Miller, *J. Chem. Phys.* **52**, 3563–3572 (1970).
25. P. Siska, *Rev. Mod. Phys.* **65**, 337–412 (1993).
26. S. Tanteri, S. D. S. Gordon, J. Zou, A. Osterwalder, *J. Phys. Chem. A* **125**, 10021–10034 (2021).
27. A. B. Henson, S. Gersten, Y. Shagam, J. Narevicius, E. Narevicius, *Science* **338**, 234–238 (2012).
28. A. Klein *et al.*, *Nat. Phys.* **13**, 35–38 (2017).
29. B. Margulis, J. Narevicius, E. Narevicius, *Nat. Commun.* **11**, 3553 (2020).
30. U. Even, J. Jortner, D. Noy, N. Lavie, C. Cossart-Magos, *J. Chem. Phys.* **112**, 8068–8071 (2000).
31. K. Luria, N. Lavie, U. Even, *Rev. Sci. Instrum.* **80**, 104102 (2009).
32. D. Koner, J. C. San Vicente Veliz, A. van der Avoird, M. Meuwly, *Phys. Chem. Chem. Phys.* **21**, 24976–24983 (2019).
33. M. Meuwly, J. M. Hutson, *J. Chem. Phys.* **110**, 8338–8347 (1999).
34. J. M. Bowman, B. Gazdy, *J. Chem. Phys.* **94**, 816–817 (1991).
35. P. Pechukas, J. C. Light, C. Rankin, *J. Chem. Phys.* **44**, 794–805 (1966).
36. B. Margulis *et al.*, *Phys. Rev. Res.* **4**, 043042 (2022).
37. B. Margulis *et al.*, Zenodo (2023); https://doi.org/10.5281/zenodo.7633162.

ACKNOWLEDGMENTS

We thank F. Gianturco for sharing preliminary cross sections that allowed us to test our own wave packet simulation code. E.N. acknowledges support from the Cluster of Excellence RESOLV. **Funding:** We gratefully acknowledge financial support from the European Research Council Advanced Grant (E.N.), the NCCR MUST and the University of Basel (M.M.), and the Deutsche Forschungsgemeinschaft (Project "Efficient Quantum Control of Molecular Rotations," grant 505622963) (C.P.K.). **Author contribution:** B.M., N.K., and E.N. designed, constructed, and conducted the experiment and analyzed the results. M.U. and M.M. designed, computed, and tested the potential energy surfaces. K.P.H. and D.M.R. wrote the scattering software with the help of A.C., A.v.d.A., and G.C.G. and calculated theoretical cross sections, which were analyzed by K.P.H., D.M.R., A.C., and C.P.K. All authors contributed to writing and revising the manuscript. **Competing interests:** The authors declare that they have no competing interests. **Data and materials availability:** All data underlying the figures are deposited at Zenodo (*37*). The information for the potential energy surfaces is available at https://github.com/MMunibas/rgh2.

SUPPLEMENTARY MATERIALS

science.org/doi/10.1126/science.adf9888
Materials and Methods
Supplementary Text
Figs. S1 to S10
Table S1
References (*38*–*51*)

Submitted 25 November 2022; accepted 8 March 2023
10.1126/science.adf9888

Tomography of Feshbach resonance states

Baruch Margulis, Karl P. Horn, Daniel M. Reich, Meenu Upadhyay, Nitzan Kahn, Arthur Christianen, Ad van der Avoird, Gerrit C. Groenenboom, Markus Meuwly, Christiane P. Koch, and Edvardas Narevicius

Science, **380** (6640), .
DOI: 10.1126/science.adf9888

Imaging all Feshbach resonances at once

Quantum scattering resonances, and Feshbach resonances in particular, are the key features of cold collisions that can fundamentally change collision outcomes. Numerous previous experiments have mainly focused on the initial channel, providing limited insight into the resonant scattering dynamics. Margulis *et al*. developed a method in which the energetics and decay channels of Feshbach resonances, formed by collisions induced by Penning ionization of metastable helium or neon atoms and the ground-state hydrogen molecule, were mapped out by ion-electron coincidence velocity map imaging with a precision of several Kelvin, enough to resolve all the final rovibrational quantum states in a single measurement. The proposed method offers a new approach to quantum state mapping of resonant collision dynamics. —YS

Science (ISSN) is published by the American Association for the Advancement of Science. 1200 New York Avenue NW, Washington, DC 20005. The title *Science* is a registered trademark of AAAS.